Quantum dots as targeted doxorubicin drug delivery nanosystems in human lung cancer cells

Monika Ruzycka (mruzycka@wum.edu.pl)
Warszawski Uniwersytet Medyczny https://orcid.org/0000-0002-2838-6625
Patrycja Kowalik
University of Warsaw, Warsaw University of Technology
Agata Kowalczyk
University of Warsaw
Piotr Bujak
Warsaw University of Technology
Anna M. Nowicka
University of Warsaw
Maria Wojewódzka
Centre for Radiobiology and Biological Dosimetry
Marcin Kruszewski
Centre for Radiobiology and Biological Dosimetry, Institute of Rural Health
Ireneusz P. Grudzinski
Medical University of Warsaw

Research

Keywords: quantum dots, doxorubicin, targeted drug delivery, lung cancer cells, cytotoxicity, genotoxicity, comet assay

Posted Date: June 26th, 2020

DOI: https://doi.org/10.21203/rs.3.rs-37874/v1

Abstract

Background Lung cancer is one of the most frequently diagnosed cancer all over the world and a leading cancer-related mortality. The therapy of lung cancer includes surgery, chemotherapy and radiatherapy and mailny depends on the type and stage of lung cancer characterized based on WHO guidelines. Althought the conventional chemotherapy is the main treatment option for small cell lung cancer (SCLC) and a common treatment for non-SCLC it is characterized with lack of specificity resulting to severe toxicities of normal cells and harmful side effects. Therefore, targeted drug delivery (TDD) systems have been used to reduce the systemic toxicity of some conventional chemotherapies in lung cancer. Quantum dots (QDs) are fascinating nanoscale crystals that can serve as nanocarriers in TDD due to their unique physicochemical properties. Therefore, in this paper, the as-desiged QDs, Ag-In-Zn-S-based nanoconjugates for selective doxorubicin (DOX) targeting to lung cancer cells were developed. The QD nanocrystals were modified with 11-mercaptoundecanoic acid (MUA), L-cysteine (Cys) and lipoic acid (LA) used as drug carriers for targeted delivery of DOX to A549 cells through conjugated folic acid (FA) a self-navigation molecule that docks to the folate receptors on cancer cells. The comprechensive physicochemical, cytotoxicity and genotoxicity studies were performed to characterise the novel QD-based nanocaries and their anticancer cargos. Results The results from FTIR, DLS and fluorescence quenching evidenced the successful attachment of FA to the QDs nanocrystals and DOX to the QDs-FA nanocarriers. UV-vis analysis determined the amount of FA and DOX covalently anchored to the QDs nanocrystal surface. Biological screeining revealed that QDs-FA-DOX nanoconjugates showed higher cytotoxicity in comparison to other forms of the synthesized QD samples, suggesting the cytotoxic effect of liberated DOX from the QD constructs. QD-MUA-FA-DOX occurred to be the most cytotoxic against A549 cells among nanoconjugates. In vitro scratch assay also revealed significant inhibition of A549 migration only due to treatment with QD-MUA-FA-DOX. Studies evidenced that all the nanoconjugates at IC 50 induced significantly more DNA breaks than that observed in non-treated cells. All in all, significant and the greatest cytotoxicity, genotoxicity together with inhibition of migratory potential of A549 cells was observed for QD-MUA-FA-DOX. Conclusion The studies show the therapeutic efficacy of DOX-loaded QD-based cargos suggesting their promising role as novel drug delivery systems navigating to folate receptors in lung cancer cells.

Background

Dynamic development of nanotechnology opened new possibilities of using some nanoscaled materials for innovative therapies and diagnostics in modern nanomedicine. Among different nanoparticles studied in biomedical sector, metal and metal oxides, dendrimers, silica- and carbon-based nanoparticles and especially quantum dots have been vigorously tested as novel theranostics (1). Quantum dots are fascinating nanoscale semiconductor crystals gaining an increasing attention in medical industry due to their unique physical and optical properties, such as small diameter ranging from 2 to 100 nm (2), size-tunable light emission (3), wide absorption/extinction coefficients and high fluorescent quantum yields (4), The surface composition of QDs may be chemically modified enhancing their water-solubility (5), suspension characteristics (6), the emission spectra and biocompatibility (2). Versatile functionalization

with biomolecules and/or drugs makes them attractive nanoplatforms to be applied in diagnostic (imaging, sensing)(3) and therapy, as they are able of side specific drug delivery to organs (6), cells and even cell components (7). Moreover, QDs are found to be a powerful tool in diagnosis and treatment, as they have great potential for simultaneous application of biosensing, imaging and therapy in nano-theranostics platforms (3).

Targeted drug cancer delivery is recently developed type of treatment having immense capability to improve cancer therapy by selective drug distribution at the tumor site at therapeutically effective concentrations along with lowering systemic toxicity and therapeutic index (8). The side specific therapeutic delivery is possible due to utility of nanoscaled materials, like QDs, that can be functionalized with self-navigating elements and therapeutic cargo. Folic acid has the properties of selective self-navigating molecule, as its receptors are frequently overexpressed on the surface of some human cancer cells. FA can be easily internalized in a nondestructive manner into cancerous cells *via* endocytic pathway that facilitates delivery of folate-conjugated anticancer drug payloads into cells in the same receptor-mediated process called a Trojan horse strategy (9–11). To date, treatments that involve folate-targeted approaches were extensively studied in context of variety of therapeutic cargos, including chemotherapeutic agents, imaging agents, oligonucleotides and DNA molecules (12). One of the widely used chemotherapeutic agent is doxorubicin, a topoisomerase inhibitor that interaction with DNA leads to growth suppression of cancer cells (13). DOX is useful for treatment of various types of cancer, including lung (14), breast (15), colon (16) and hematologic cancers (17). Even there are many cases of successful treatments and cancer attenuation with DOX, its frequent clinical use induces multidrug resistance (MDR) and severe side effects like cardiotoxicity and ototoxicity, as well as liver abnormalities, raised level of uric acid in the blood and heart failure. To overcome those adverse effects, DOX was proposed to be encapsulated and/or chemically conjugated to nanoparticles (18). Therefore, in this paper Ag-In-Zn-S quantum dots conjugated with FA and DOX were synthesized. For further functionalization with FA and DOX surface of QD was modified with 11-mercaptoundecanoic acid (MUA), L-cysteine (Cys) and lipoic acid (LA) ligands. As a result, nine compounds were developed including QD-MUA, QD-Cys, QD-LA nanocrystals, QD-MUA-FA, QD-Cys-FA, QD-LA-FA nanocarriers and QD-MUA-FA-DOX, QD-Cys-FA-DOX and QD-LA-FA-DOX nanoconjugates. The physicochemical characterization of synthesized QDs was obtained using transmission electron microscopy (TEM), fourier transformation infrared spectroscopy (FTIR), fluorescence spectroscopy, UV-VIS spectroscopy, dynamic light scattering (DLS) and by zeta potential (ZP) analysis. The cytotoxic effect was evaluated on adenocarcinomic human alveolar basal epithelial cells (A549) based on Alamar Blue and Colony Forming Efficiency (CFE) assays. The migratory potential of A549 cells exposed to the newly synthesized QDs was estimated based on *in vitro* wound healing assay (scratch assay). Genotoxicity expressed as induction of DNA breaks was assessed using the single cell gel electrophoresis assay (comet assay).

Materials And Methods

Materials

Sodium dihydrogen phosphate, disodium hydrogen phosphate, sodium chloride, potassium chloride (all from POCH, Poland), silver nitrate (99%), indium(III) chloride (98%), zinc stearate (technical grade), 1-dodecanethiol (DDT, 98%), sulfur (99%), 1-octadecene (ODE, 90%), oleylamine (OLA, 70%), 11-mercaptoundecanoic acid (MUA, 95%), dimethyl sulfoxide (DMSO), L-cysteine (Cys, > 97%), lipoic acid (LA, > 99%), *N*-hydroxy-succinimide (NHS), *N*-(3-dimethylaminopropyl)-*N*-ethylcarbodiimide hydrochloride (EDC), doxorubicin hydrochloride (DOX) and folic acid (FA > 97%) were all purchased from Sigma-Aldrich, USA. Reagents and chemicals used in the nanoconjugate synthesis and in the cytotoxicity tests were of the highest purity available and used as received.

Synthesis of Ag-In-Zn-S nanocrystals

In the synthesis of Ag-In-Zn-S nanocrystals and primary ligand exchange procedures earlier described in the literature were followed.[19,20] All operations were carried out under a constant dry argon flow. Silver nitrate (0.03 g, 0.17 mmol), indium(III) chloride (0.13 g, 0.59 mmol), zinc stearate (0.87 g, 1.37 mmol for QD_{green}), and DDT (0.20 g, 1.00 mmol) were mixed with ODE (15 mL) in a three-neck flask. The mixture was heated to 150 °C until a homogenous solution was formed. Then sulphur (0.015 g, 0.47 mmol) dissolved in 1 mL of OLA was quickly injected into the reaction solution. The temperature was increased to 180 °C and the mixture was kept at this temperature for 60 min. Then the mixture was cooled to room temperature and toluene (20 mL) was added. Further, the reaction mixture was centrifuged and isolated black precipitate was separated. The supernatant was treated with 30 mL of acetone resulting in precipitation of the desired fraction of nanocrystals. The nanocrystals were separated by centrifugation (7000 rpm, 5 min) and then redispersed in toluene.

Ligand exchange for 11-mercaptoundecanoic acid (MUA). A mixture of MUA (0.5 g, 2.3 mmol) and NaOH (0.1 g, 2.5 mmol) in water (10 mL) was stirred and heated at 50 °C until a homogenous solution was formed. Then the toluene dispersion (10 mL) of nanocrystals prepared as described above was injected into this solution. The as-obtained two-phase mixture was heated at 80 °C for 8 h under an argon atmosphere. After cooling, the reaction mixture was centrifuged to obtain a complete phase separation and the solid and organic phases were discarded. Water phase was then mixed with 20 mL of acetone, which led to precipitation of nanocrystals. After centrifugation, the nanocrystals were redispersed in 10 mL of water.

Ligand exchange for L-cysteine (Cys). A mixture of L-cysteine (3.0 g, 24.8 mmol), NaOH (1.5 g, 37.5 mmol) in water (10 mL) was stirred and heated at 40 °C until a homogenous solution was formed. Then the toluene dispersion (10 mL) of nanocrystals prepared as described above was injected into this solution. The as-obtained two-phase mixture was heated at 40 °C for 4 h under an argon atmosphere. After cooling, the reaction mixture was centrifuged to obtain a complete phase separation, and the organic phase was discarded. Water solution was then mixed with 20 mL of acetone, which led to the precipitation of nanocrystals. After centrifugation, the nanocrystals were redispersed in 10 mL of water.

Ligand exchange for lipoic acid (LA). A sodium borohydride (0.02 g, 0.53 mmol) was added to the solution of lipoic acid (0.2 g, 0.97 mmol) and NaOH (0.05 g, 1.25 mmol) in 10 mL of water and stirred at

40 °C under argon atmosphere for 1 h. Then the toluene dispersion (10 mL) of nanocrystals prepared as described above was injected into this solution. The mixture was stirred at 40 °C for 4 h and at room temperature for 8 h. The mixture was centrifuged to obtain a complete phase separation and the organic phase was discarded. Water solution was then mixed with 20 mL of acetone, which led to the precipitation of nanocrystals. After centrifugation, the nanocrystals were redispersed in 10 mL of water. The TEM images of the nanocrystals are presented in Fig. 1A. Table 1 QD shows nanocrystals parameters before and after ligand exchange.

Table 1
Precursor molar ratios (silver nitrate/indium chloride/zinc stearate/DDT/sulfur in 1 mL of OLA) and characteristics of Ag-In-Zn-S nanocrystals: before and after ligands exchange for MUA, Cys and LA. TEM was used for size studies.

Ligand	$Ag/In/Zn/S_{DDT}/S_s$	Ag/In/Zn/S	Size[a] (nm)	PL[b] (nm)	Q.Y.[c] (%)
initial ligands*	1.0/3.5/8.1/5.8/2.6	1.0/1.5/7.8/17.0	3.2 ± 0.4	543	48.0
MUA		1.0/1.2/5.6/9.4	3.1 ± 0.6	576	25.0
initial ligands*	1.0/3.5/8.1/5.8/2.6	1.0/1.5/7.8/17.0	3.2 ± 0.4	543	48.0
Cys		1.0/6.8/14.3/154.2	3.1 ± 1.0	524	16.0
initial ligands*	1.0/3.5/8.1/5.8/2.6	1.0/1.5/7.8/17.0	3.2 ± 0.4	543	48.0
LA		1.0/1.0/8.8/25.1	3.0 ± 0.7	540	28.0

*stearic acid and 1-aminooctadecane; [a]average diameter of nanocrystals (n = 200) determined by TEM; [b]maximum of the photoluminescence band; [c]photoluminescence quantum yield.

Synthesis of QD-FA-DOX nanoconjugates

The FA was attached to QD nanocrystals *via* EDC/NHS coupling reaction, as shown in Scheme 1. Briefly, 5 mL of QD (10 $mg \cdot mL^{-1}$) was diluted with 5 mL of solution containing 40 mM EDC and 10 mM NHS and left under stirring for 1 h. The FA (5 mg; 10 mL) solution was prepared separately in PBS with addition of 1% DMSO. The prepared solution of FA was added to the flask containing the activated QD nanocrystals and incubated overnight with stirring in ThermoMixer Eppendorf® at the room temperature in the flask protected from light. After that, the mixtures of each type of QD-FA nanocarriers were dialyzed against distilled water during 5 days to remove unbound FA. An amount of the unbounded FA present in the supernatant of dialysis was determined by UV-vis spectroscopy. The difference of the absorbance of the FA band (*ca.* 280 nm) between the initial solution and supernatant was the basis for the calculation the amount of FA attached to the QD nanocrystals.

QD-FA-DOX nanoconjugates were prepared by conjugation of DOX with QD-FA nanocarriers *via* amino groups. To the 1 mM solution of DOX in citrate buffer the NHS/EDC-activated QD-FA nanocarriers were

added, see Scheme 1. The reaction was continued at room temperature overnight. Then the mixtures of each type of QD-FA-DOX nanoconjugates were dialyzed against distilled water during 5 days to remove unbound DOX. Finally, obtained nanoconjugates were diluted with water to the QD concentration 1 $mg \cdot mL^{-1}$. The amount of DOX conjugated with QD-FA nanocarriers was determined according to the same procedure applied in the calculations of FA anchored to the QD nanocrystals. It was found that *ca.* 400 μM of DOX was attached to each type of QD-FA nanocarriers (1 $mg \cdot mL^{-1}$).

Applied characterization methods

Transmission electron microscopy (TEM). TEM analysis were performed on a Zeiss Libra 120 electron microscope operating at 120 kV. The elemental analysis was carried out with a multichannel Quantax 400 EDS system with 125 eV xFlash Detector 5010, Bruker using 15 kV electron beam energy.

Fourier transformation infrared spectroscopy (FTIR). FTIR spectroscopy was used to confirm the successful conjugation of DOX and FA compounds to QD. The pellets were prepared from a mixture of 300 mg of spectrally pure KBr and *ca.* 1.0 mg of the nanoconjugates (QD-MUA-FA-DOX, QD-Cys-FA-DOX and QD-LA-FA-DOX) and pure components (QD-MUA, QD-Cys, QD-LA, FA and DOX). The spectra were acquired in a transmission mode on Perkin Elmer System 2000 spectrophotometer with the spectral resolution of 4 cm^{-1}.

Fluorescence spectroscopy. Fluorometric measurements were performed by means of Scinco-FS2 spectrofluorimeter (Scinco, South Korea) with low volume (200 μL) optical cuvette (Product no. 16.100 F/Q/10 from Starna Stientific, Co, UK) compatible in terms of size and aperture position with the apparatus. Excitation wavelength was adjusted at 350 nm in compliance to preliminary measurements. The fluorescence spectra were recorded from 360 nm to 690 nm with the maximum emission wavelength *ca.* 535, 550 and 543 nm for QD-MUA, QD-Cys and QD-LA, respectively. The other parameters like slits width (excitation: 5 nm, emission 5 nm), PMT voltage (600 V) scan speed (600 $nm \cdot min^{-1}$), were adjusted experimentally in order to obtain the best sensitivity and linearity in respected range of concentration of used compounds.

UV-vis spectroscopy. The UV-vis spectra were obtained with a PerkinElmer spectrometer, model Lambda 25 at temperature 21 °C in the quartz cuvette of 1-cm length.

Dynamic light scattering (DLS) and zeta potential (ZP) analysis. DLS and ZP measurements were performed with a Zetasizer nano series apparatus (Malvern) with a He-Ne (4 mW) laser at 632.8 nm. The experiments were carried out in buffer at 25 °C, at least five times, with three freshly prepared samples.

Cell line

The A549 (ATCC® CCL-185™) cell line was obtained from American Type Culture Collection (ATCC, Manassas, VA, USA). The cells were cultivated in a 5% CO_2 atmosphere at 37 °C in CO_2 incubator (Memmert, Schwabach, Germany). The cells were grown as adherent monolayer in F-12K Medium

(Kaighn's Modification of Ham's F-12 Medium, Gibco, Paisley, UK), supplemented with 10% FBS (Fetal Bovine Serum, Gibco, Paisley, UK) and antibiotics: streptomycin, 50 $\mu g \cdot mL^{-1}$; amphotericin B, 1.25 $\mu g \cdot mL^{-1}$; gentamicin 50 $\mu g \cdot mL^{-1}$; penicillin, 50 $U \cdot mL^{-1}$ (Gibco, Paisley, UK).

Cytotoxicity assessment

Cytotoxicity assessment was performed based on Alamar Blue and Colony Forming Efficacy assays.

Alamar Blue assay. The Alamar Blue assay was carried out according to manufacturer's instruction (Alamar Blue™ Cell Viability Reagent, ThermoFisher Scientific, Life Technologies Corporation, Eugene, Oregon, USA). A549 cells were trypsinized (0.25% trypsin/EDTA solution, Gibco, Paisley, UK) and plated in 96-well plates (Falcon, Corning, Durham, USA) at a density of 10^5 cells per well. 24 h after cell adhesion, A549 cells were exposed to increasing concentrations (0.1, 1, 5, 10, 25, 50, 100 $\mu g \cdot mL^{-1}$) of QD-MUA, QD-Cys, QD-LA, QD-MUA-FA, QD-Cys-FA, QD-LA-FA, QD-MUA-FA-DOX, QD-Cys-FA-DOX, QD-LA-FA-DOX and free DOX, which were further incubated for 24 h. The control cells were incubated with media. After incubation, control medium and investigated compounds were removed, then the cells were rinsed twice with PBS and 100 µL of Alamar Blue solution (10% [v/v] solution of Alamar Blue dye in fresh medium) was transferred to each well. Following 3 h incubation (37 °C, 5% CO_2, 90% humidity), the Alamar Blue fluorescence was quantified at the excitation and emission wavelength of 570 and 600 nm, respectively, using an Epoch microplate reader (BioTek). The viability was expressed as fluorescence counts in the presence of test compound as a percentage of that in the control.

Colony Forming Efficacy assay. On the first day, the A549 cells (400/dish) were seeded in 3 mL of fresh complete medium in each 60 mm Petri dish. After 24 h of incubation (37 °C, 5% CO2, 90% humidity), the cells were treated with the most promising QDs nanocojugates, i.e. which revealed significant cytotoxicity in Alamar Blue assay and free DOX. The concentration values selected based on the Alamar Blue data applying values close to IC_{50} concentration calculated for the as-obtained QDs nanoconjugates. Therefore, the concentrations of QD-MUA-FA-DOX were 1 $\mu g \cdot mL^{-1}$ and 5 $\mu g \cdot mL^{-1}$, QD-Cys-FA-DOX were 10 $\mu g \cdot mL^{-1}$ and 25 $\mu g \cdot mL^{-1}$, QD-LA-FA-DOX were 5 $\mu g \cdot mL^{-1}$and 10 $\mu g \cdot mL^{-1}$ and DOX were 0.1 $\mu g \cdot mL^{-1}$ and 1 $\mu g \cdot mL^{-1}$, respectively. Three replicates per each concentration were performed. Positive control (sodium chromate, Na_2CrO_4, 100 µM), negative control (medium) and solvent control (PBS) were done in parallel studies. The cells were treated for 72 h. When the time elapsed, the incubated medium with added nanoconjugates or DOX were removed and replaced with complete fresh culture medium. After the next 72 h, the cells were fixed and stained with fixing solution of 10% v/v of formaldehyde in PBS and staining solution of 10% v/v of Giemsa in ultrapure water, respectively. Dishes were air-dried before colony counting. The colonies were counted under the stereoscopic microscope (OPTI Tech Scientific).

In vitro **scratch assay**

The scratch assay was carried out based on the protocol published by Liang et al. [21] A549 cells (1.5×10^5 cells/well) were seeded in 24-well plates to grow in a monolayer for 24 h. After that time, a "scratch" was

created with a sterile 20–200 µL pipette tip in each well. The detached cells were removed by washing twice with PBS. Afterwards, 250 µL of both, fresh medium without FBS and the most promising QDs nanocojugates at final concentration of IC_{50} were added and incubated for 72 h. The control was fresh medium without FBS and positive control was medium with 10% FBS. Three replicates per concentration were performed. The scratches were observed under a phase-contrast microscope and photographed at the reference point. The scratch closure was monitored at 0, 24, 48, and 72 h of experiment using a microscope (Delta Optical NIB-100) at 4·magnification. The analysis of the scratch images was performed using the ImageJ which calculates the scratch area. The migration of cells toward the scratch is expressed as percentage of scratch closure:

1

$$\%\ of\ wound\ closure = \frac{A_{t=0\ h} - A_{t=\Delta\ h}}{A_{t=0\ h}} \cdot 100\%$$

where, $A_{t=0\ h}$ is the area of wound measured immediately after scratching, and $A_{t=\Delta\ h}$ is the area of wound measured 24, 48 or 72 h post scratching.[22]

The comet assay

For the comet assay (single cell gel electrophoresis), A549 cells (2.5×10^5 cells/well) were seeded in 24-well plates to grow in a monolayer. For 24 h after cell adhesion, the cells were exposed to final concentration of IC_{50} and IC_{10} of the most promising QDs nanoconjugates and free DOX, which were further incubated for 24 h. Control cells were incubated with media and PBS. Positive control were control cells X-irradiated (2 Gy) in an ice water bath, with the use of a Smart200 (Yxlon) defectoscope operating at 200 kV and 4.5 mA, with 3 mm Al filtration, at a dose rate of 1.14 Gy/min. A549 cells were trypsinized and an aliquot of cells was mixed with an equal volume of 2% low melting point agarose (Type VII) and put on a microscope slide pre-coated with 0.5% regular agarose (Type I-A). The slides were immediately placed in lysis solution and afterwards placed on a horizontal gel electrophoresis unit filled with fresh electrophoresis buffer (1 mM Na_2EDTA and 300 mM NaOH, pH > 13 for 40 min for DNA unwinding). Next, electrophoresis was performed (1.2 $V \cdot cm^{-1}$, 30 min, 10 °C), then the slides were washed with 0.4 M Tris, pH 7.5 (3 × 5 min) and stained with DAPI, 50 µL, 1 $\mu g \cdot mL^{-1}$. Images of 100 randomly selected comets per slide were captured at 200 × magnification using a fluorescence microscope (Labophot-2, Nikon, Japan) equipped with Pulnix TM765 CCD camera (JAI, Japan). Image analysis of the data was performed by the Comet v.3.0 software (Kinetic Imaging Ltd., UK).

Statistical analysis

Data are presented as the mean value ± standard deviation (SD). The study was conducted in at least three independent runs. The graphs were prepared in GraphPad Prism 8 (GraphPad Software, Inc, La Jolla, USA). The statistical analysis was performed with Statistica and GraphPad Prism software using an unpaired t-test or the Mann – Whitney U test. $P < 0.05$ was considered statistically significant.

Results And Discussions

Qualitative features of the FTIR spectra of the QD-FA nanocarriers and QD-FA-DOX nanoconjugates.

Exact information about the functional groups involved in the conjugation process between QD nanocrystals and FA and DOX would be given by comparison of FTIR spectra of pure QDs, FA and DOX with the QDs-FA nanocarriers and QDs-FA-DOX nanoconjugates. The FTIR spectra of pure components, nanocarriers and nanoconjugates are presented in Fig. 2. For all studied QD nanocrystals (Fig. 2A) the characteristic stretching vibrations: of C = O at *ca.* 1560 cm^{-1} and O-H in-plane band at *ca.* 1410 cm^{-1} in carboxylate groups are visible. As shown in Fig. 2B, in the case of pure folic acid the stretching vibration of C = O appears at 1696 cm^{-1}, while the band at 1607 cm^{-1} relates to the bending mode of NH– vibration. The bands between 1513 and 1485 cm^{-1} are attributed to band of the phenyl and pterin ring.[23] In turn, the FTIR spectrum of DOX indicated characteristics bands at 1730 cm^{-1} (C = O stretch, ketone), 1630 cm^{-1} (C = O stretch), 1282.7 cm^{-1} (C – O–C, stretch), 1114 cm^{-1} (C – O stretch, tertiary alcohol), 1070 cm^{-1} (C – O stretch, secondary alcohol), and 988 cm^{-1} (C – O stretch, primary alcohol).[24,25] The FTIR spectrum of QD-FA nanocarriers presented in Fig. 2C shows the bands characteristic for QD nanocrystals and FA. The effect of conjugation of the QDs with FA *via* amide bond can be characterized by the amide I and amide II bands. The amide I band corresponds mainly to the C = O stretching vibration of the amide groups and occurs in the region 1600–1700 cm^{-1}. The amide II band (1480–1575 cm^{-1}) comes from N-H bending (40–60%) and C-N stretching (18–40%) vibrations (26, 27) After covalent (*via* amide bond, Fig. 2D) conjugation of doxorubicin to QD-FA nanocarriers several important features characteristic for this drug appeared on the FTIR spectrum of QD-FA-DOX nanoconjugates. Additionally, a small shift in the amide I and amide II positions were observed with respect to pure components. Moreover, the presence of the bands characteristic for the drug, at *ca.* 1300 cm^{-1} confirms the successful attachment of DOX.

QD fluorescence quenching studies as a proof of QD and FA conjugation.

The interactions of FA with each type of QD nanocrystals were examined using fluorescence titrations. The effect of FA concentration on the emission spectra of appropriate QDs is illustrated in Fig. 3. Examined QD nanocrystals are characterized by emission maximum at *ca.* 573, 545 and 551 for QD-MUA, QD-Cys and QD-LA, respectively. In the all cases the addition of FA led to the gradual fluorescence decrease with increasing concentration of FA in the solutions. In particular, for the highest FA content (5 μM), the fluorescence intensities were quenched to *ca.* 80 and 75% of original value of QD-MUA and QD-Cys or QD-LA, respectively. The QD-FA interactions can be quantitatively described by the quenching constant (K_{SV}) of the QD-FA nanocarriers according to the Stern-Volmer Eq. (28–30):

2

$$\frac{I_0}{I} = 1 + K_{SV} \cdot C_{FA}$$

where C_{FA} is the molar concentration of FA, I_0 and I are the fluorescence intensity of QD in the absence and in the presence of FA, respectively. K_{SV} values were calculated from the slopes of the each plot $I_0/I = f(C_{FA})$ and were equal to $(3.7 \pm 0.3)\cdot10^4$, $(5.7 \pm 0.4)\cdot10^4$ and $(6.7 \pm 0.5)\cdot10^4$ M^{-1} for QD-MUA-FA, QD-Cys-FA and QD-LA-FA, respectively. The Stern-Volmer plots were linear (see insets in Fig. 3), so only one type of quenching process occurs, either static or dynamic one (31, 32). The simplest way to distinguish the static from dynamic quenching is the monitoring of K_{SV} changes in the function of temperature (31). In the case of an increase of the K_{SV} value with temperature the dynamic quenching takes place. Opposite behavior of K_{SV} *vs.* T is typical for static quenching. For all QD-FA nanocarriers the decrease of K_{SV} values were observed with increasing temperature. Such behavior suggests that the static quenching took place and, subsequently, the quenching constants could be considered as the association constant.

Size and physical stability of QD-FA nanocarriers and QD-FA-DOX nanoconjugates.

Size of the QD nanocrystals, QD-FA nanocarriers and QD-FA-DOX nanoconjugates has been considered as one of qualitative parameters proving the successful conjugation process. Based on DLS studies, the diameter of the QD nanocrystals dispersed in PBS buffer was in the range 11–19 nm depending on the surface ligand type (Fig. 4).

It should be stressed that the hydrodynamic diameter of QD nanocrystals is significantly higher than those determined from TEM images (see Table 1). The highest QD nanoconjugates diameter was observed for the lipoic acid as a surface ligand. This can be explained by the different number of zinc atoms and in consequence the greater number of ligands that stabilize such ions. Probably two coordination spheres of ligands exist. The first sphere contains ligands directly bounded to the surface, the second sphere includes free ligands that are in balance with the first sphere ligands. During the bioconjugation process the size of QD nanocrystals increased along with another modification of their surface by FA and DOX.

The zeta potential was exploited as one of the decisive factors of the QD nanocrystals, QD-FA nanocarriers and QD-FA-DOX nanoconjugates. The obtained ZP values are showed in Table 2. The ZP plays an essential role in QD-FA-DOX nanoconjugates stability. The higher ZP value (positive or negative) the more stable dispersion is. In general, nanoparticles with zeta potential values greater than positive 30 mV or less than negative 30 mV have high degrees of stability. Dispersions with less than + 25 mV or greater than − 25 mV zeta potential value will eventually agglomerate due to interparticle interactions, including van der Waals and hydrophobic interactions, and hydrogen bonding. In the study, the smallest ZP values were observed for QD-FA-DOX nanoconjugates for all tested types of QD. This fact suggests that such behavior might be favorable for the release of DOX from nanoconjugates in the cell culture medium.

Table 2
Zeta potential values for QD nanocrystals, QD-FA nanocarriers and QD-FA-DOX nanoconjugates obtained in PBS buffer.

	MUA	Cys	LA
QD	-23.3 ± 2.4	-24.3 ± 3.5	-10.9 ± 1.2
QD-FA	-34.1 ± 2.6	-27.8 ± 2.7	-13.2 ± 2.2
QD-FA-DOX	-15.5 ± 3.5	-17.2 ± 1.9	-6.2 ± 1.1

Quantitative analysis of QD-FA nanocarriers and QD-FA-DOX nanoconjugates.

The amount of FA and DOX covalently anchored to QD nanocrystal surface was determined from UV-vis analysis (Table 3).

Table 3
Mass of FA and DOX anchored to 1 g of each type of QD nanocrystals.

	m_{FA}/1 g QD [mg]		m_{DOX}/1 g QD [mg]	
	exp.	theor.	exp.	theor.
QD-MUA	11	28	46	56
QD-Cys	13	50	54	102
QD-LA	9	21	39	42

It should be noted, that these values correspond to *ca.* 30–40% of maximal value for FA, most likely represents the lower limit of surface coverage. It is probably because of steric reasons, where some FA molecules lie on the ligand layer at QD surface and efficiently block the conjugations sites. The situation is much better in the case of DOX; the mass of DOX covalently attached to the QD-FA nanocarriers corresponds to *ca.* 50–80% of maximal value for FA and most likely represents the higher limit of surface coverage. Probably DOX molecules were anchored to the QD-FA nanocarriers *via* amide bond formed with FA molecules, as well as directly with the ligand at the QD surface. In the calculations of maximal mass of FA and DOX it was assumed that DOX molecules on the surface of QD are 2D close packed, and its maximal number per one QD molecule is:

$$\frac{S_{QD}}{S_{DOX}} = \frac{4\pi r^2}{\pi r^2} = 205, 175 \text{ and } 550 \text{ molecules for QD-MUA, QD-Cys and QD-LA, respectively;}$$

$$\frac{S_{QD}}{S_{FA}} = \frac{4\pi r^2}{\pi r^2} = 132, 113 \text{ and } 355 \text{ molecules for QD-MUA, QD-Cys and QD-LA, respectively.}$$

Taking into account the composition of studied QD nanocrystals: QD-MUA ($Ag_{1.00}In_{1.20}Zn_{5.60}S_{9.40}$), QD-Cys ($Ag_{1.00}In_{6.80}Zn_{14.30}S_{154.20}$), QD-LA ($Ag_{1.00}In_{1.00}Zn_{8.80}S_{25.10}$) the densities of QDs were determined on the basis of density of its components and are presented in Table 4. Knowing the volume of a single QD molecule, the number of QDs in 1 g and the FA or DOX masses that correspond to the maximal number of QD, the maximal (theoretical) mass of FA and DOX covalently attached to the 1 g of QD nanocrystals were estimated.

Table 4
Diameter (φ), radius (r), density (ρ), volume of single QD molecules (V_{QD}) and the number of QD molecules (N_{QD}).

	φ [nm]	r [nm]	ρ [g·cm^{-3}]	V_{QD} [cm^{-3}]	N_{QD} in 1 g
QD-MUA	11.5	5.7	4.51	$7.75 \cdot 10^{-19}$	$2.86 \cdot 10^{17}$
QD-Cys	14.0	7.0	2.63	$6.23 \cdot 10^{-19}$	$6.10 \cdot 10^{17}$
QD-LA	18.8	9.4	3.60	$3.48 \cdot 10^{-18}$	$7.99 \cdot 10^{16}$
φ: QD nanoparticle diameter; r: QD nanoparticle radius; ρ: QD density determined on the basis of density of its components; V_{QD}: volume of a single QD molecule (); N_{QD}: number of QD molecules in 1 g					

Cytotoxicity assessment

One of the most important objectives of our study was to assess the cytostatic activity of the as-obtained quantum dot nanoplatforms loaded with and without doxorubicin. Relevant tests were conducted on A549 cells with commonly used anti-cancer drug doxorubicin alone serving as reference compound.

Alamar Blue. In the present study, A549 cells were *in vitro* treated with QD-MUA, QD-Cys, QD-LA nanocrystals, QD-MUA-FA, QD-Cys-FA, QD-LA-FA nanocarriers and QD-MUA-FA-DOX, QD-Cys-FA-DOX and QD-LA-FA-DOX nanoconjugates for 24 h. The results of the cell viability measurements showed the lowest Alamar Blue reduction for A549 cells treated with the QD-Cys-FA-DOX nanoconjugates (Fig. 5D). QD-MUA-FA-DOX was found to be the most cytotoxic among studied QD nanoconjugates (Fig. 5D) since its IC_{50} value was 1.7 μg·mL^{-1} (95% CI 0.9 to 2.7 μg·mL^{-1}), while IC_{50} values for QD-Cys-FA-DOX and QD-LA-FA-DOX were 10.5 μg·mL^{-1} (95% CI: 7.7 to 13.8 μg·mL^{-1}) and 5.5 μg·mL^{-1} (95% CI: 4.0 to 7.3 μg·mL^{-1}), respectively. The successful application of Ag-In-Zn-S QDs with MUA as linker in anticancer therapy has been also recently reported by Pilch et al (33). They used QD-MUA as a carrier of bisacridine derivatives (UAs) for enhancement its cytotoxicity toward cancerous cells. As a result, they observed increased therapeutic efficiency of UAs toward lung (H460) and colon (HCT116) cancer cells preserving the protective effect on normal cells.

No cytotoxic effect was observed for all QDs nanocrystals apart from QD-MUA at the highest studied concentration (Fig. 5A). The significant cytotoxic effect of QD-MUA was observed due to treatment of 100 $\mu g \cdot mL^{-1}$, similarly to its derivative form (QD-MUA-FA) obtained by conjugation of FA (Fig. 5A). In both cases, about 40% loss of the cell viability was noted in comparison to preceding studied concentration (50 $\mu g \cdot mL^{-1}$). In other recent studies, no cytotoxicity of QD-MUA on cancerous cells H460, HCT116 and normal MRC-5 and CCD 841CoN cells was reported (33). Interestingly, the cytotoxicity of MUA in the absence of QDs core was investigated by Hoshino et al. who revealed severe toxic effect at doses grater then 100 $\mu g \cdot mL^{-1}$ within 12 h of treatment (34). Note that FA functionalized QDs was found to have an ambiguous effect on the cytotoxicity of studied cells. The treatment with the highest applied concentration of QD-Cys-FA slightly increased the A549 cells viability (Fig. 5B), whereas the treatment with QD-LA-FA did not influence the cells regardless of the tested concentrations (Fig. 5C). It was previously reported that FA plays a great role as a ligand in targeted cancer therapy, however, excessive FA supplementation may lead to neocarcinogenesis and some cancers progression (35–37). A549 cells were also treated with free doxorubicin. The Alamar Blue assay revealed a quite different profile of free DOX and DOX conjugated quantum dots as IC_{50} of DOX was established at 0.8 $\mu g \cdot mL^{-1}$ and IC_{50} of QD-MUA-FA-DOX (QD with the highest cytotoxic effect) at 1.7 $\mu g \cdot mL^{-1}$. Note that the 1.7 $\mu g \cdot mL^{-1}$ of QD-MUA-FA-DOX contains 0.08 $\mu g \cdot mL^{-1}$ of DOX, what is 10 times less than the IC_{50} value of free DOX. One has to be noted that the QD-based nanocarriers contain lower amount of DOX as compared to free DOX used in the cytotoxicity assay (Table 3).

Colony Forming Efficiency assay. Colony Forming Efficiency assay serves for assessment of cytotoxicity induced both by chemicals and nanomaterials, based on the ability of a single cell to form a colony.[38] The assay gives rise to the information of the number of colonies being an important parameter of tumor growth and progression. It is also considered to be a promising tool to study nanomaterials as is a label-free (non-colorimetric, non-fluorescent), therefore limits the possibility of the occurrence of interferences especially associated with optical detection (39).

In this case, the CFE assay was used as a confirmation of growth inhibition of A549 by the most promising QDs nanoconjugates at the concentrations established based on the Alamar Blue test that revealed significant the cytotoxic effect, i.e. all the QDs nanoconjugates with FA and DOX. The control and solvent control revealed the plating efficiency to be more than 45% (Fig. 6). As a rule, the colonies of more than 50 cells should be counted in the CFE assay (38), however, in our experiment the selected concentrations of QDs nanoconjugates strongly suppressed A549 growth leading to the reduction of cells and the size of the colonies with more than 50 cells within. As a consequence, no colonies of 50 cells were evidenced (beside the both controls). Nevertheless, there were many incidents of small colonies containing 2 to 10 cells (Fig. 6), therefore, the comparative analysis was only limited to this group. The colonies containing 11–25 cells and 25–50 cells were also investigated, however occurred in a large minority. All things considered, this result indicates that all QDs nanoconjugates strongly inhibited the capability of A549 cells to grow. Interestingly, among the colonies formed, a quite different shape of colonies was found as compared to respective controls (Fig. 6).

The CFE assay revealed that QDs nanoconjugates treatment enhances cell death in a concentration dependent manner as the reductions in the size and number of colonies were observed (Fig. 7). The statistical analyses revealed significant differences ($P < 0.05$) in all compared groups. The greatest decrease in the number of colonies containing 2 to 10 cells ($P < 0.0001$) was observed for QD-Cys-FA-DOX after treatment with 25 $\mu g \cdot mL^{-1}$ in comparison to 10 $\mu g \cdot mL^{-1}$.

In vitro **scratch assay**

Cells migration is a multistep process fundamental to normal biological, however, also pathological events such as cancer metastasis (40). In order to determine the migratory/invasive potential of A549 cells after the exposition to QDs nanoconjugates, the *in vitro* scratch assay was performed. The method depends on registration the time upon which the artificial gap created by the tip will be closed by the cells from the edge of the newly created gap. The comparison of the images at the beginning and regular intervals during cell migration to close the scratch determines the rate of cell migration (Fig. 8).

In vitro scratch assay revealed statistically significant inhibition ($P < 0.05$) of A549 cells due to QD-MUA-FA-DOX treatment at IC_{50} within 24 h and 72 h post-scratching in comparison to control (Fig. 9). Other studied QDs or free DOX did not revealed any significant inhibition of A549 cells migration comparing to control. Considerable wound healing rate of A549 after treatment with DOX was also reported by Sheng et al. due to cells treatment with 1 μM (0.54 $\mu g \cdot mL^{-1}$) at 24 h of incubation (41) and Li et al. due to treatment with 4 $\mu g \cdot mL^{-1}$ at 48 h of incubation (42).

The Comet Assay

The Comet assay was applied to determine the genotoxicity of as-synthesized QDs-FA-DOX nanoconjugates. The assay enables the detection of DNA damage in a single cell by measurement the chromatin release in the process of high pH electrophoresis proceeded by exposition to lysis detergents and high salts. The chromatin release resembling comet structure is the effect of genotoxic insult indicating on DNA strand breaks. The representative “comets” are counted under the fluorescence microscope giving rise to the information about the DNA damage, which is estimated based on the intensity of the comet tail relative to the head (43, 44). The *in vitro* comet assay on A549 cells treated with QD-MUA-FA-DOX, QD-Cys-FA-DOX, QD-LA-FA-DOX or DOX as a reference was carried out after 24 h of exposure. The statistically significant differences in DNA damage between the cells treated with IC_{50} and untreated control were observed for all synthesized QDs-FA-DOX nanoconjugates, but not for DOX alone (Fig. 10). No difference from the control was observed for the compounds at concentration of IC_{10}. The representative comets were shown in Fig. 11.

Doxorubicin is well known substrate for multidrug resistance protein, especially ABCB1 protein (also known as a MDR1 protein) (45, 46). Since ABCB1 is a transmembrane protein, the extracellularly added doxorubicin is exported directly from the vicinity of outer membrane thus does not even enter the cell interior (46). This likely explains the neglectable genotoxicity of DOX alone, as the compound must reach

nucleus and DNA to become toxic. On the other hand, FA present of the nanoconjugates surface apparently dodges the ABCB1 action due to the ligand-receptor interactions and enabled DOX delivery to the cytoplasm. Moreover, FA containing nanoconjugates might be able to deliver DOX to the cell's nucleus, as proved for ultrasmall gold nanoparticles conjugated with lipoic acid/FA/DOX complex (47). Our results confirm this observation as genotoxicity of FA/DOX containing nanoconjugates was higher that the genotoxicity of DOX alone. Moreover, referring to QD-MUA-FA-DOX genotoxicity its linker (MUA) alone was also previously reported to be genotoxic at doses greater than or equal to 50 $\mu g \cdot mL^{-1}$ with 2 h of treatment (34, 48).

Conclusions

Nanoconjugates of DOX and FA with Ag-In-Zn-S quantum dots modified with three different drug carriers (MUA, Cys, LA) were synthesized and characterized. The physicochemical properties of all QDs nanocrystals, QDs-FA nanocarriers and QDs-FA-DOX nanoconjugates were investigated using TEM, FTIR, DLS, ZP, fluorescence and UV-vis spectroscopy. The TEM analyses enabled us to evaluate the size of QD nanocrystals, QD-FA nanocarriers and QD-FA-DOX nanoconjugates, while the DLS analyses allowed to establish the hydrodynamic diameter of the as-synthesized QDs. The results from FTIR evidenced the successful attachment of folic acid to QDs nanocrystals and doxorubicin to QDs-FA nanocarriers. FA conjugation to QDs nanocrystals was also proven by QD fluorescence quenching. UV-vis analysis revealed the actual mass of folic acid and doxorubicin covalently anchored to QDs nanocrystal surface. The data from zeta potential investigation demonstrated that the smallest ZP value was obtained as follow by QD-Cys-FA-DOX, QD-MUA-FA-DOX and QD-LA-FA-DOX nanoconjugates indicating on the favorable release of DOX from nanoconjugates in the cell medium. Among those three nanoconjugates, QD-Cys and QD-MUA nanocarriers attached the highest amount of FA and DOX having facilitated docking to cancer cells through folate receptors and providing more DOX into the cells. The Alamar Blue cytotoxicity assessment proved the above assumptions as the greatest cytotoxic effect was observed for QD-MUA-FA-DOX, QD-LA-FA-DOX and QD-Cys-FA-DOX (QDs presented according to increasing *IC* values). Among nanoconjugates, QD-MUA-FA-DOX occurred to be the most cytotoxic against A549 cells, what may be explained by mild itself MUA cytotoxicity. In turn, CFE assay revealed complete cells inhibition by all nanoconjugates at concentrations close to IC_{50} values determined in Alamar Blue assay. The *in vitro* scratch assay also revealed significant inhibition of A549 migration only due to treatment with QD-MUA-FA-DOX at IC_{50}. On the other hand, the comet test demonstrated significant genotoxicity of all QDs nanoconjugates at concentrations relevant to IC_{50}. Higher genotoxicity was also observed for free DOX at IC_{50}, however not statistically significant suggesting the higher genotoxicity of FA/DOX containing nanoconjugates than that of DOX alone. Having in mind the decrease of the well-known adverse effects of DOX the proposed QDs perfectly fulfill their roles both due to the targeted delivery of DOX to the lung cancer cells, thus reduction its systemic cytotoxicity and the diminution of DOX availability to other healthy tissues while maintaining its therapeutic effectiveness.

Ethics approval and consent to participate

Not applicable.
Consent for publication
Not applicable.
Availability of data and material
The datasets used and/or analysed during the current study are available from the corresponding author on reasonable request.

Declarations

Ethics approval and consent to participate

Not applicable.

Consent for publication

Not applicable.

Availability of data and material

The datasets used and/or analysed during the current study are available from the corresponding author on reasonable request.

Competing interests

There are no conflicts to declare.

Funding

Not applicable.

Authors' contributions

MR performed biological research, analyzed and interpreted final results and was a major contributor in writing the manuscript. PK synthesized the QD nanocrystals, performed and analyzed fluorescence experiments. AK synthesized the QD-FA and QD-FA-DOX nanoconjugates, performed and analyzed FTIR experiments, participated in writing of original draft. PB designed and supervised the QD synthesis and photoluminescence experiments, participated in writing of original draft. AMN designed and reviewed the chemical part of experiments, performed and analyzed DLS and ZP experiments, performed quantitative analysis of QD-FA nanocarriers and QD-FA-DOX nanoconjugates, wrote the manuscript. MW performed comet assay and wrote the manuscript. MK analyzed and interpreted biological data and participated in writing of original draft. IPG analyzed and interpreted final results and discussion. All the authors read and approved the final manuscript.

Acknowledgements

The authors are grateful to Zuzanna Wichrzycka for help in organizing the CFE and wound healing experiments.

Authors' information

[1]Faculty of Pharmacy, Medical University of Warsaw, Banacha 1, 02-097 Warsaw, Poland, [2]Faculty of Chemistry, University of Warsaw, Pasteura 1, 02-093 Warsaw, Poland, [3]Faculty of Chemistry, Warsaw University of Technology, Nowakowskiego 3, 00-664 Warsaw, Poland, [4]Centre for Radiobiology and Biological Dosimetry, Institute of Nuclear Chemistry and Technology, Dorodna 16, 03-195 Warsaw, Poland, [5]Department of Medical Biology and Translational Research, Institute of Rural Health, Jaczewskiego 2, 20-090 Lublin, Poland

References

1. 10.1016/B978-0-12-815886-9.00004-8
   Ha S-W, Weiss D, Weitzmann MN, Beck GR. S.-W, in Nanobiomaterials in Clinical Dentistry (Second Edition), eds. Subramani K, Ahmed W, Elsevier, 2019, DOI: https://doi.org/10.1016/B978-0-12-815886-9.00004-8, pp. 77–112.
2. Peynshaert K, Soenen SJ, Manshian BB, Doak SH, Braeckmans K, De Smedt SC, et al. Coating of Quantum Dots strongly defines their effect on lysosomal health and autophagy. Acta Biomater. 2017;48:195–205.
3. Matea CT, Mocan T, Tabaran F, Pop T, Mosteanu O, Puia C, et al. Quantum dots in imaging, drug delivery and sensor applications. Int J Nanomed. 2017;12:5421–31.
4. Abbasi E, Kafshdooz T, Bakhtiary M, Nikzamir N, Nikzamir N, Nikzamir M, et al. Biomedical and biological applications of quantum dots. Artificial Cells Nanomedicine Biotechnology. 2016;44(3):885–91.
5. Bilan R, Fleury F, Nabiev I, Sukhanova A. Quantum Dot Surface Chemistry and Functionalization for Cell Targeting and Imaging. Bioconjug Chem. 2015;26(4):609–24.
6. Hardman R. A toxicologic review of quantum dots: toxicity depends on physicochemical and environmental factors. Environmental health perspectives. 2006;114(2):165–72.
7. Wegner KD, Hildebrandt N. Quantum dots: bright and versatile in vitro and in vivo fluorescence imaging biosensors. Chem Soc Rev. 2015;44(14):4792–834.
8. Salahuddin N, Galal A. in Nanostructures for Cancer Therapy, Ficai A, Grumezescu AM, Elsevier, editors, 2017, DOI: https://doi.org/10.1016/B978-0-323-46144-3.00004-0, pp. 87–128.
9. Zhang J, Zhao X, Xian M, Dong C, Shuang S. Folic acid-conjugated green luminescent carbon dots as a nanoprobe for identifying folate receptor-positive cancer cells. Talanta. 2018;183:39–47.
10. Sosnik A. Chapter 1 - From the “Magic Bullet” to Advanced Nanomaterials for Active Targeting in Diagnostics and Therapeutics. In: Sarmento B, das Neves J, editors. Biomedical Applications of Functionalized Nanomaterials: Elsevier; 2018. p. 1–32.

11. Patel NR, Piroyan A, Ganta S, Morse AB, Candiloro KM, Solon AL, et al. In Vitro and In Vivo evaluation of a novel folate-targeted theranostic nanoemulsion of docetaxel for imaging and improved anticancer activity against ovarian cancers. Cancer Biol Ther. 2018;19(7):554–64.
12. Kumar P, Huo P, Liu B. Formulation Strategies for Folate-Targeted Liposomes and Their Biomedical Applications. Pharmaceutics. 2019;11(8):381.
13. Kumar A, White J, James Christie R, Dimasi N, Gao C, in Annual Reports in Medicinal Chemistry, ed. Goodnow R. A., Academic Press, 2017, vol. 50, pp. 441–480.
14. Hong Y, Che S, Hui B, Yang Y, Wang X, Zhang X, et al. Lung cancer therapy using doxorubicin and curcumin combination: Targeted prodrug based, pH sensitive nanomedicine. Biomed Pharmacother. 2019;112:108614.
15. Lovitt CJ, Shelper TB, Avery VM. Doxorubicin resistance in breast cancer cells is mediated by extracellular matrix proteins. BMC Cancer. 2018;18(1):41.
16. Lin Y-Q, Zhang J, Liu S-J, Ye H. Doxorubicin Loaded Silica Nanoparticles with Dual Modification as a Tumor-Targeted Drug Delivery System for Colon Cancer Therapy. J Nanosci Nanotechnol. 2018;18(4):2330–6.
17. Au KM, Balhorn R, Balhorn MC, Park SI, Wang AZ. High-Performance Concurrent Chemo-Immuno-Radiotherapy for the Treatment of Hematologic Cancer through Selective High-Affinity Ligand Antibody Mimic-Functionalized Doxorubicin-Encapsulated Nanoparticles. ACS Central Science. 2019;5(1):122–44.
18. Gu Y-J, Cheng J, Man CW-Y, Wong W-T, Cheng SH. Gold-doxorubicin nanoconjugates for overcoming multidrug resistance. Nanomed Nanotechnol Biol Med. 2012;8(2):204–11.
19. Gabka G, Bujak P, Giedyk K, Ostrowski A, Malinowska K, Herbich J, et al. A Simple Route to Alloyed Quaternary Nanocrystals Ag–In–Zn–S with Shape and Size Control. Inorg Chem. 2014;53(10):5002–12.
20. Gabka G, Bujak P, Kotwica K, Ostrowski A, Lisowski W, Sobczak JW, et al. Luminophores of tunable colors from ternary Ag–In–S and quaternary Ag–In–Zn–S nanocrystals covering the visible to near-infrared spectral range. Physical Chemistry Chemical Physics. 2017;19(2):1217–28.
21. Liang CC, Park AY, Guan JL. In vitro scratch assay: a convenient and inexpensive method for analysis of cell migration in vitro. Nat Protoc. 2007;2(2):329–33.
22. Zhang J, Rana S, Srivastava RS, Misra RDK. On the chemical synthesis and drug delivery response of folate receptor-activated, polyethylene glycol-functionalized magnetite nanoparticles. Acta Biomater. 2008;4(1):40–8.
23. Stanishevsky AV, Styres C, Yockell-Lelievre H, Yusuf N. Nanostructured carbon beads–properties and biomedical applications. J Nanosci Nanotechnol. 2011;11(10):8705–11.
24. Kanwal U, Bukhari NI, Rana NF, Rehman M, Hussain K, Abbas N, et al. Doxorubicin-loaded quaternary ammonium palmitoyl glycol chitosan polymeric nanoformulation: uptake by cells and organs. Int J Nanomedicine. 2019;14:1–15.

25. Coates J. Encyclopedia of Analytical Chemistry. Chichester: ed. R. A. M, editor, John Wiley&Sons Ltd; 2000. pp. 10815–37. DOI:10.1002/9780470027318.a5606.
26. Thomas YKGJ, Infrared and Raman spectroscopy (part C), E.G. Brame, J.G. Grasselli, editors, New York, 1977.
27. Pyle AM, Rehmann JP, Meshoyrer R, Kumar CV, Turro NJ, Barton JK. Mixed-ligand complexes of ruthenium(II): factors governing binding to DNA. J Am Chem Soc. 1989;111(8):3051–8.
28. Trends, Research and Technologies
Biomedical Engineering
Olsztynska S, Komorowska M. Biomedical Engineering: Trends, Research and Technologies, IntechOpen, 2011.
29. Li N, Ma Y, Yang C, Guo L, Yang X. Interaction of anticancer drug mitoxantrone with DNA analyzed by electrochemical and spectroscopic methods. Biophys Chem. 2005;116(3):199–205.
30. Lakowicz JR. Principles of fluorescence spectroscopy. Baltimore: Springer; 2010.
31. Zhong W, Yu JS, Huang W, Ni K, Liang Y. Spectroscopic studies of interaction of chlorobenzylidine with DNA. Biopolymers. 2001;62(6):315–23.
32. Pilch J, Matysiak-Brynda E, Kowalczyk A, Bujak P, Mazerska Z, Nowicka AM, et al. New Unsymmetrical Bisacridine Derivatives Noncovalently Attached to Quaternary Quantum Dots Improve Cancer Therapy by Enhancing Cytotoxicity toward Cancer Cells and Protecting Normal Cells. ACS Applied Materials & Interfaces. 2020.
33. Hoshino A, Fujioka K, Oku T, Suga M, Sasaki YF, Ohta T, et al. Physicochemical Properties and Cellular Toxicity of Nanocrystal Quantum Dots Depend on Their Surface Modification. Nano Lett. 2004;4(11):2163–9.
34. 35.
35. Pieroth R, Paver S, Day S, Lammersfeld C. Folate and Its Impact on Cancer Risk. Curr Nutr Rep. 2018;7(3):70–84.
36. Petersen LF, Brockton NT, Bakkar A, Liu S, Wen J, Weljie AM, et al. Elevated physiological levels of folic acid can increase in vitro growth and invasiveness of prostate cancer cells. BJU Int. 2012;109(5):788–95.
37. Bendale Y, Bendale V, Paul S. Evaluation of cytotoxic activity of platinum nanoparticles against normal and cancer cells and its anticancer potential through induction of apoptosis. Integrative Medicine Research. 2017;6(2):141–8.
38. Jessica Ponti AK-O, Hedvig Norlén SA, Cristina Andreoli AB, Sylvie Chevillard I, De Angelis S-TC, Igchun Eom KF, Douglas Gilliland MG, Grollino MG, et al. Interlaboratory comparison study of the Colony Forming Efficiency assay for assessing cytotoxicity of nanomaterials.: European Commission; 2014.
39. Jonkman JE, Cathcart JA, Xu F, Bartolini ME, Amon JE, Stevens KM, et al. An introduction to the wound healing assay using live-cell microscopy. Cell adhesion migration. 2014;8(5):440–51.

40. Sheng W, Mao H, Wang C, Yang N, Zhang Z, Han J. Dehydrocostus Lactone Enhances Chemotherapeutic Potential of Doxorubicin in Lung Cancer by Inducing Cell Death and Limiting Metastasis. Medical science monitor: international medical journal of experimental clinical research. 2018;24:7850–61.
41. Li L, He S, Yu L, Elshazly EH, Wang H, Chen K, et al. Codelivery of DOX and siRNA by folate-biotin-quaternized starch nanoparticles for promoting synergistic suppression of human lung cancer cells. Drug Deliv. 2019;26(1):499–508.
42. Collins AR. The comet assay for DNA damage and repair: principles, applications, and limitations. Molecular biotechnology. 2004;26(3):249–61.
43. Stice SA, Beedanagari SR, Vulimiri SV, Bhatia SP, Mahadevan B. Mahadevan. in Biomarkers in Toxicology (Second Edition), ed. Gupta RC. Academic Press, 2019, DOI: https://doi.org/10.1016/B978-0-12-814655-2.00044-X, pp. 807–821.
44. Bosch I, Croop J. P-glycoprotein multidrug resistance and cancer. Biochimica et Biophysica Acta (BBA) - Reviews on Cancer. 1996;1288(2):F37-F54.
45. Takara K, Sakaeda T, Okumura K. An update on overcoming MDR1-mediated multidrug resistance in cancer chemotherapy. Curr Pharm Design. 2006;12(3):273–86.
46. Dzwonek M, Załubiniak D, Piątek P, Cichowicz G, Męczynska-Wielgosz S, Stępkowski T, et al. Towards potent but less toxic nanopharmaceuticals – lipoic acid bioconjugates of ultrasmall gold nanoparticles with an anticancer drug and addressing unit. RSC Advances. 2018;8(27):14947–57.
47. Jamieson T, Bakhshi R, Petrova D, Pocock R, Imani M, Seifalian AM. Biological applications of quantum dots. Biomaterials. 2007;28(31):4717–32.

Figures

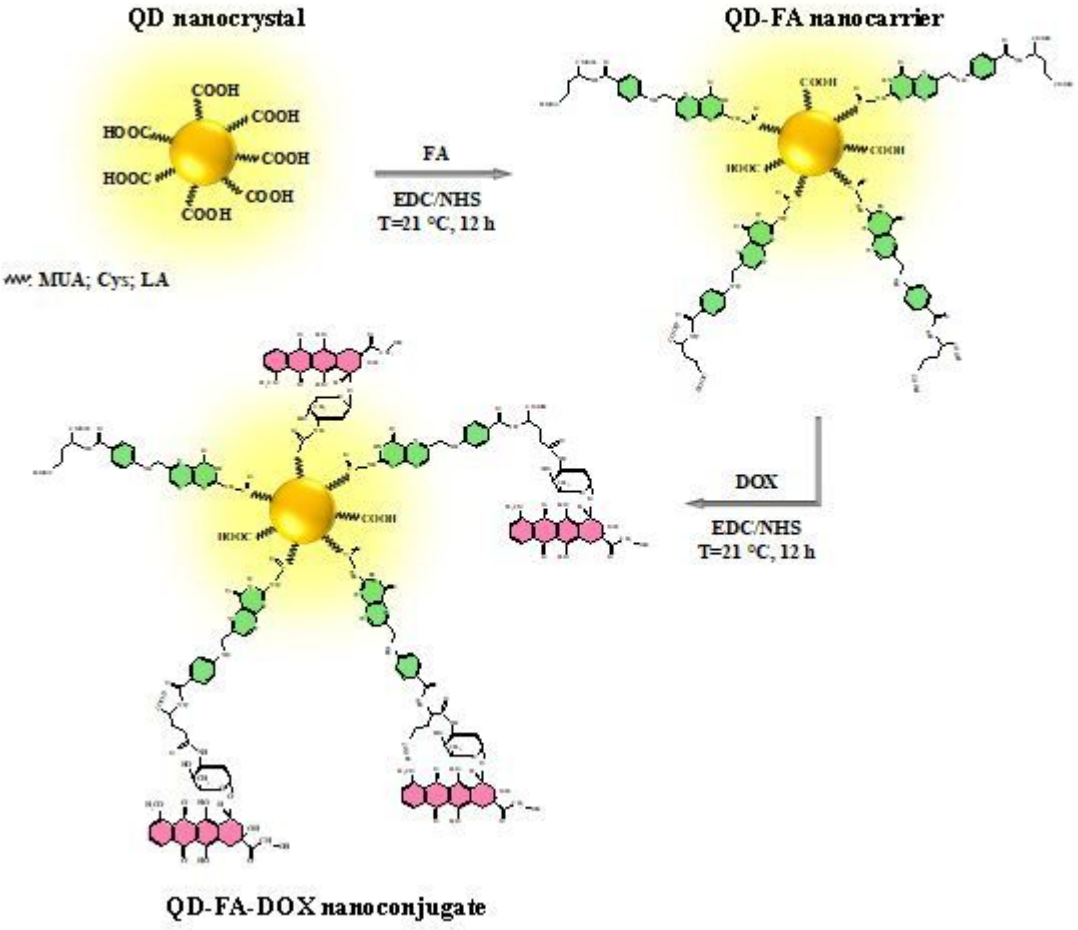

Figure 1

Scheme 1: Scheme of the synthesis of the QD-FA nanocarriers and QD-FA-DOX nanoconjugates.

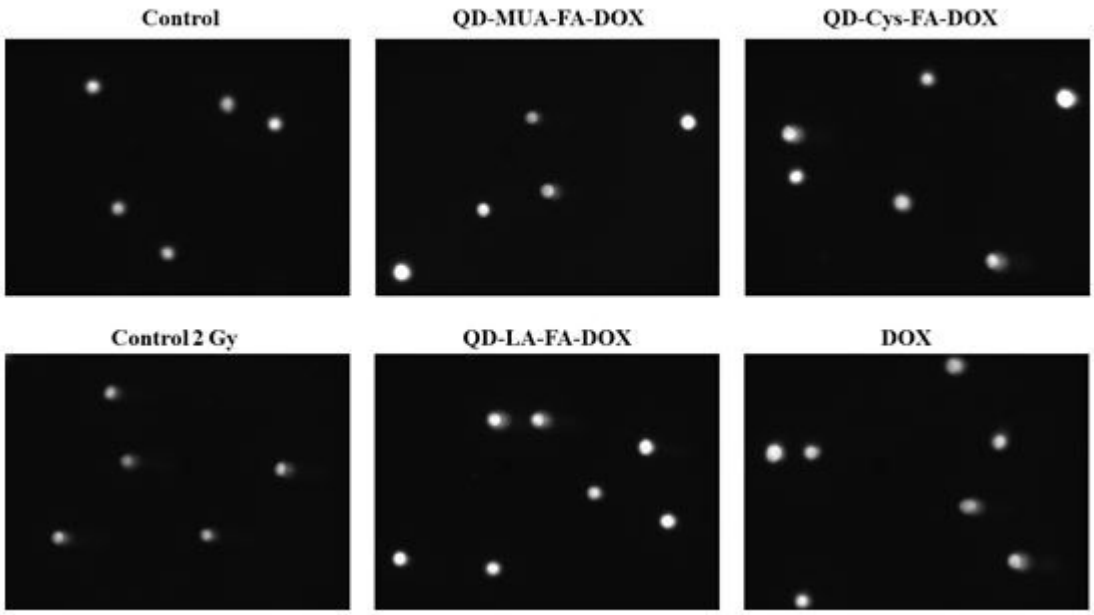

Figure 2

DNA damage of A549 cells after 24 h of treatment with the compounds at IC50 detected by the comet assay. Images come from a fluorescent microscope.

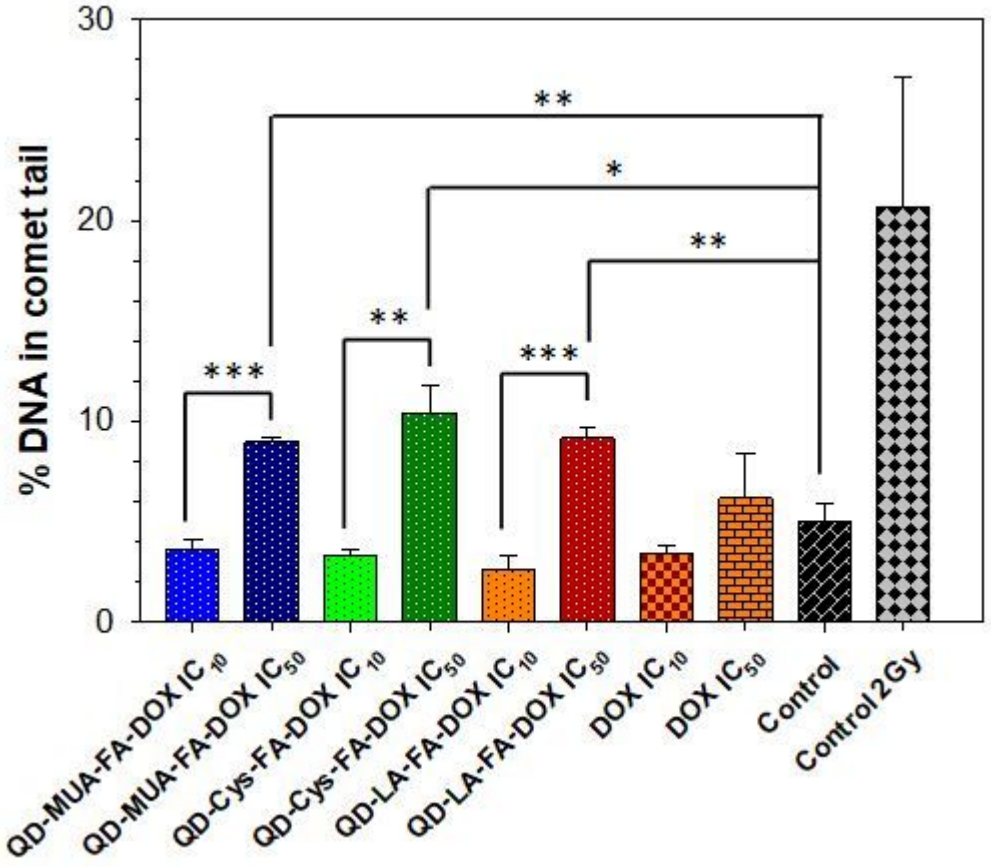

Figure 3

Percent of DNA damage in A549 cells after treatment with QD-MUA-FA-DOX (QD1), QD-Cys-FA-DOX (QD2), QD-LA-FA-DOX (QD3) and DOX at IC10 and IC50. *P < 0.05, **P <0.01, ***P < 0.001 and ****P < 0.0001, between studied concentrations.

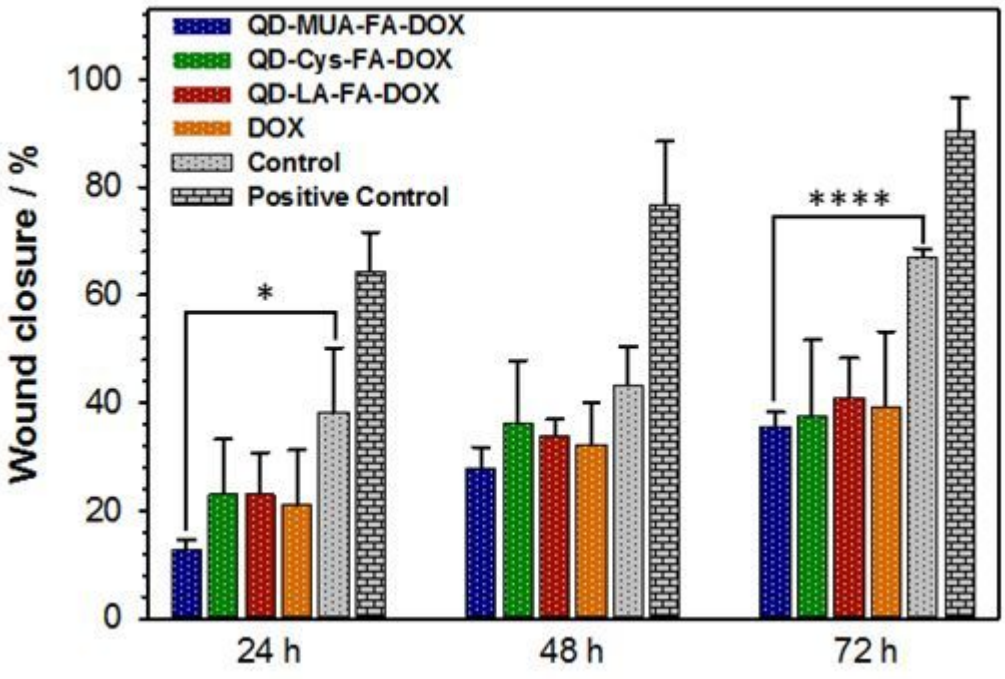

Figure 4

The percentage of wound closure area plotted over time for QD-MUA-FA-DOX, QD-Cys-FA-DOX, QD-MUA-FA-DOX and free DOX at final concentration of IC50. Data are presented as mean ± SD. *P < 0.05, **P <0.01, ***P < 0.001 and ****P < 0.0001, between studied concentrations.

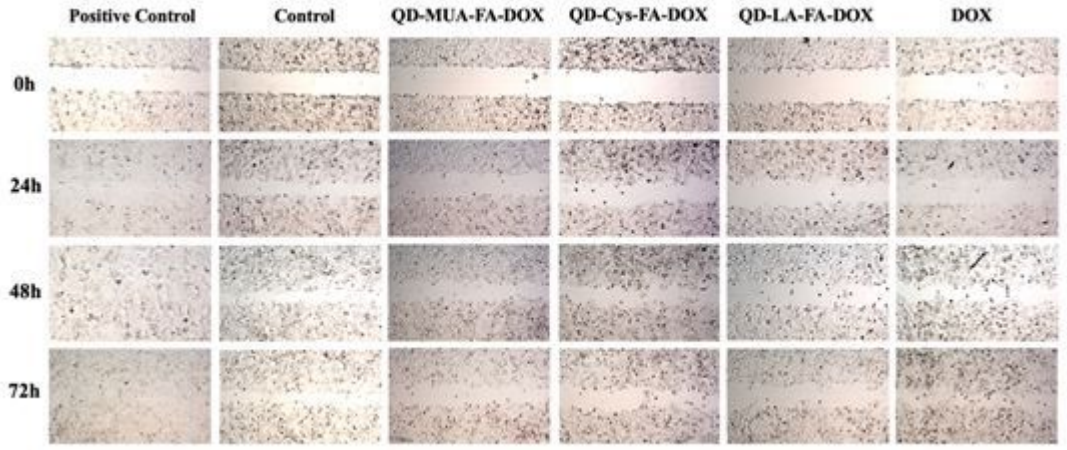

Figure 5

Effect of QD-MUA-FA-DOX, QD-Cys-FA-DOX, QD-MUA-FA-DOX and DOX on A549 migratory potential in vitro. Images were acquired at 0, 24, 48 and 72 h.

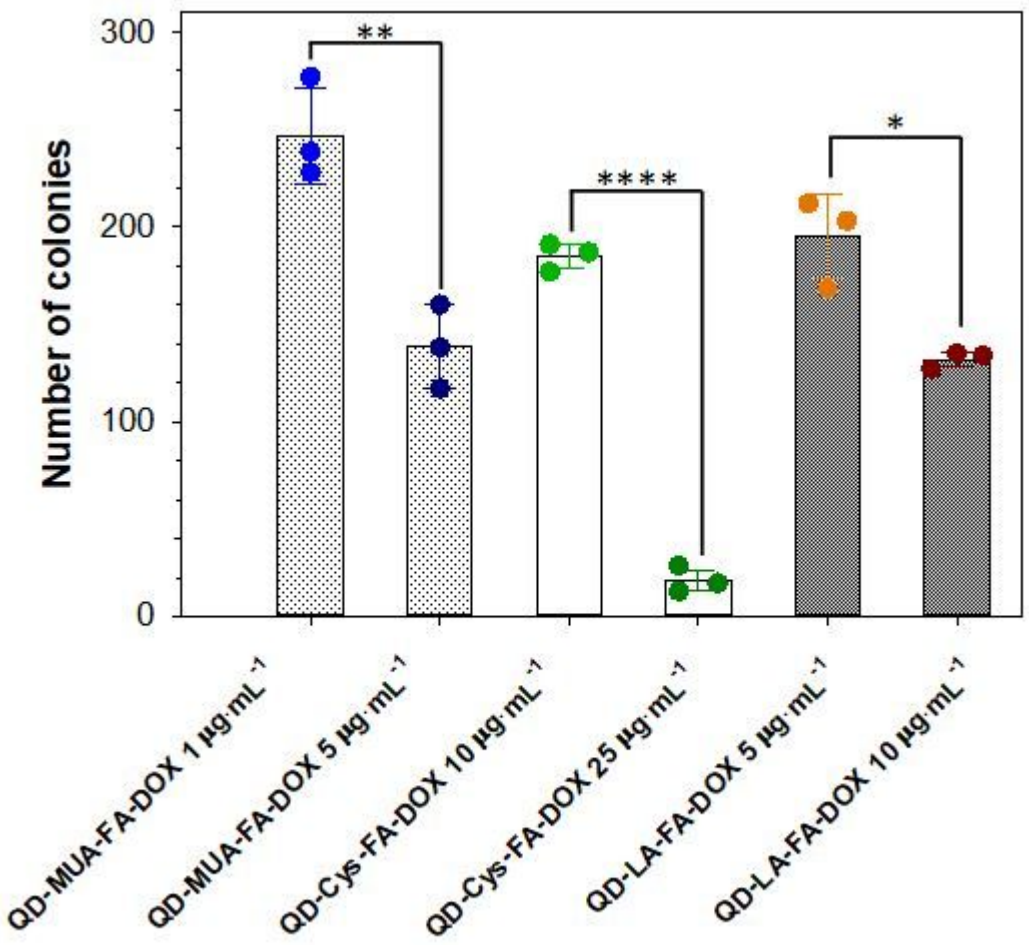

Figure 6

Number of colonies built of 2 to 10 cells of human lung carcinoma cells (A549) treated with QD-MUA-FA-DOX, QD-Cys-FA-DOX, and QD-LA-FA-DOX. Data from three independent experiments. *P < 0.05, **P < 0.01, ***P < 0.001 and ****P < 0.0001, between studied concentrations.

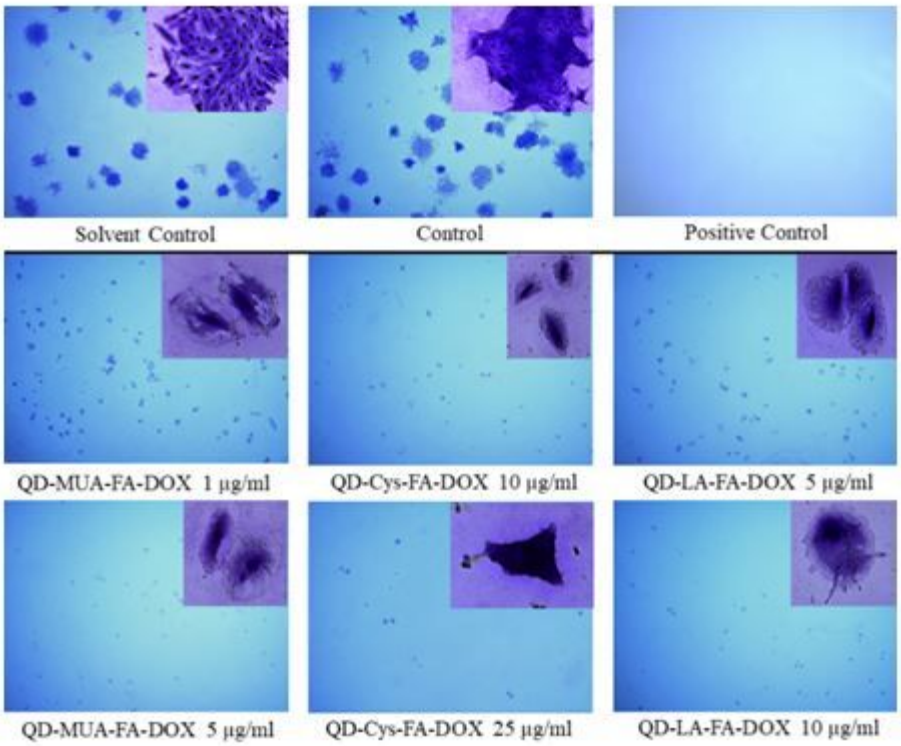

Figure 7

The representative microscopic images of A549 from CFE assay. Images are performed under the converted microscope Delta Optical NIB-100 (10xmagnification) and stereoscopic microscope Opti-Tech Scientific (2xmagnification).

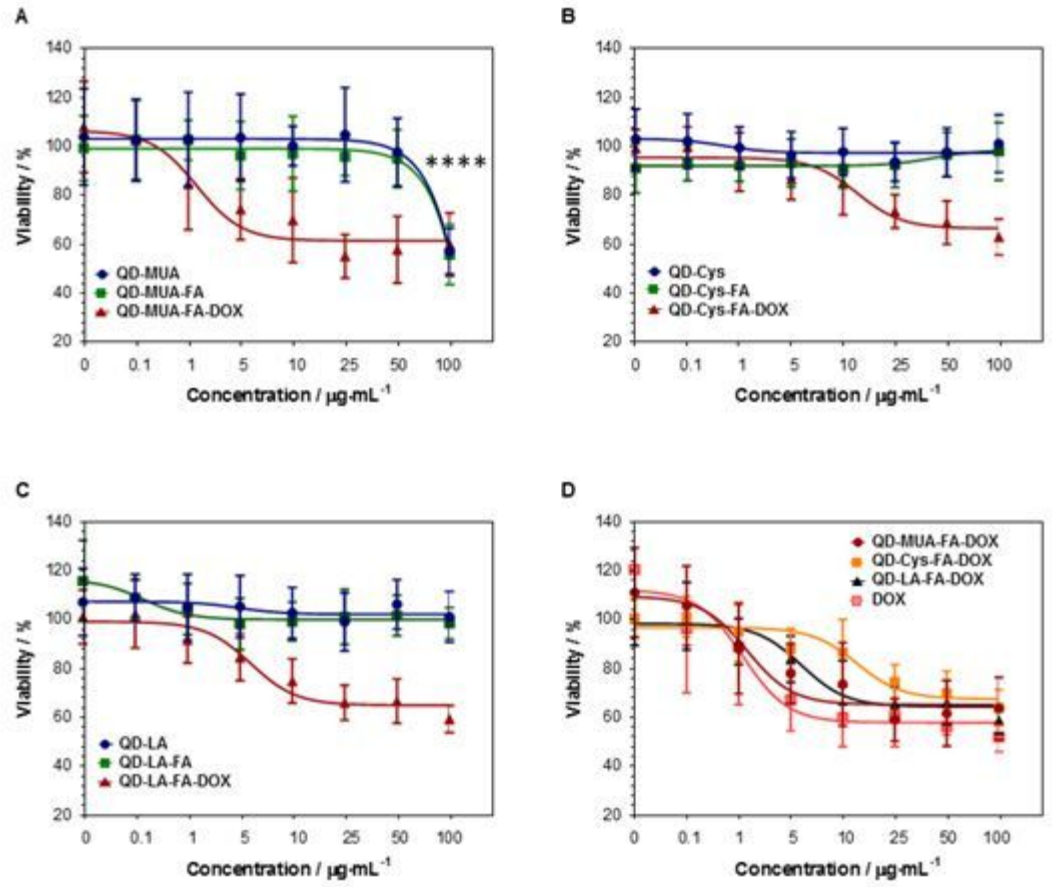

Figure 8

Viability of human lung carcinoma cells (A549) treated with QDs coated with A) MUA, B) Cys, C) LA, and D) QDs functionalized with FA and DOX and free DOX. Data are from three independent experiments. ****P < 0.0001 versus A549 cells treated with 50 µg·mL-1 of QD-MUA and QD-MUA-FA.

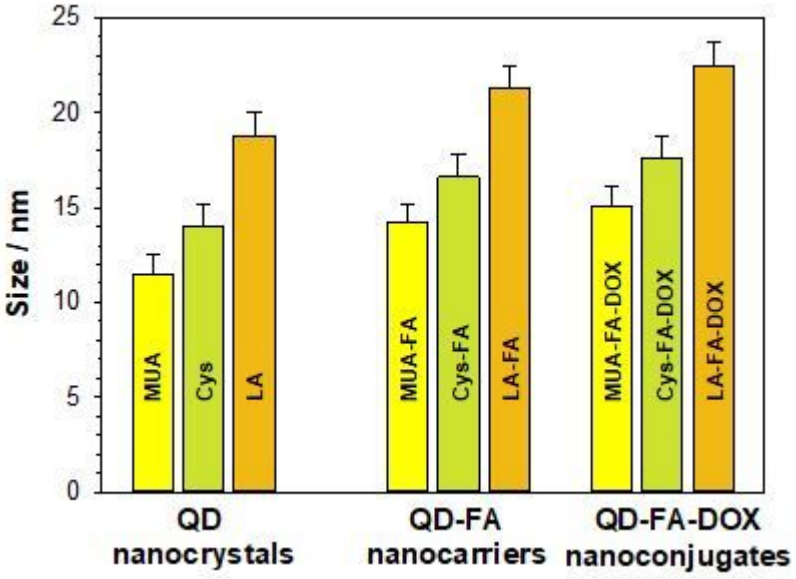

Figure 9

Mean size of QD nanocrystals, QD-FA nanocarriers and QD-FA-DOX nanoconjugates dispersed in PBS buffer based on DLS studies.

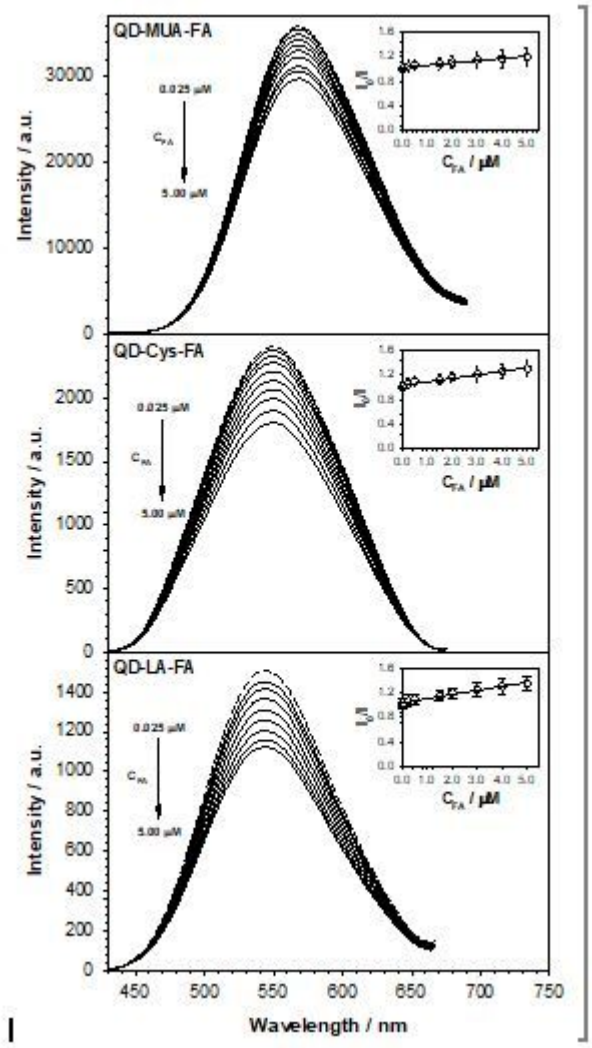

Figure 10

Fluorescence quenching of QDs by FA in 0.02 M PBS buffer of pH 7.4. Insets: Stern-Volmer plots of QD quenching fluorescence as a function of FA concentrations. Experimental conditions: CQD = 1 mg·mL-1; CFA = 0.025; 0.05; 0.25; 0.5; 1.5, 2, 3, 4 and 5 μM.

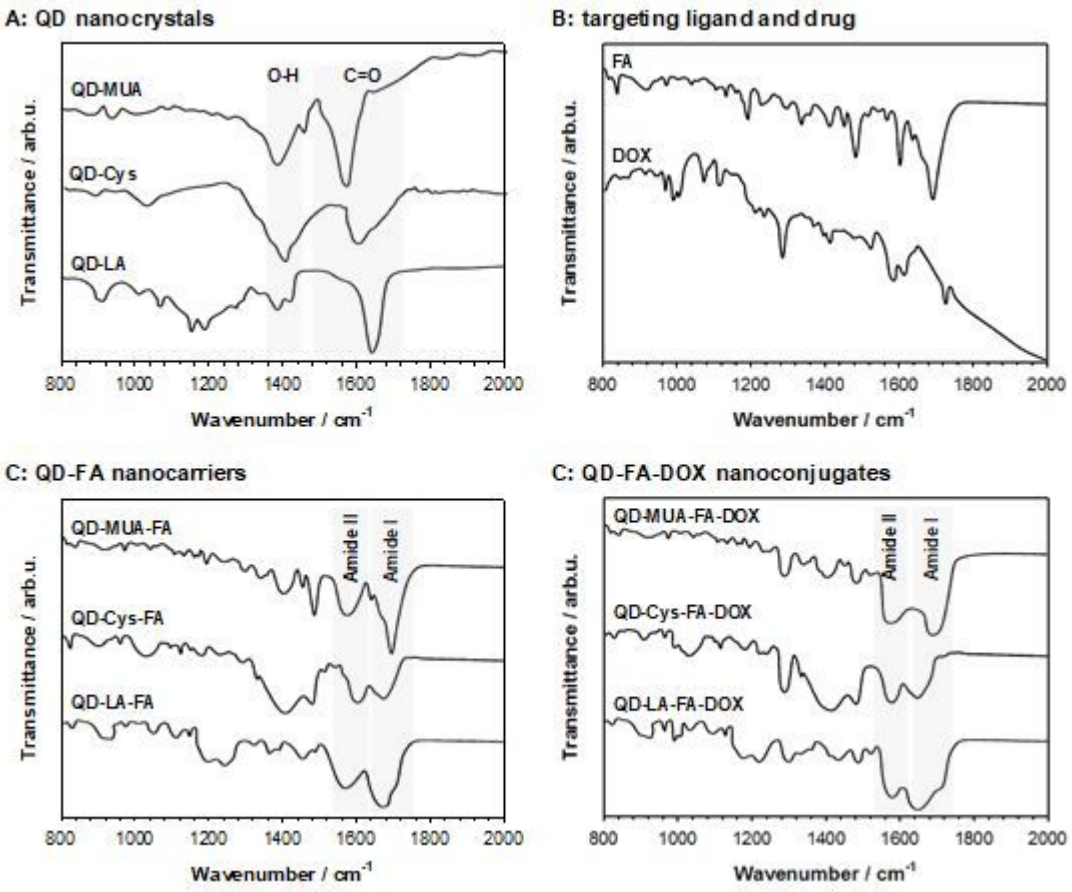

Figure 11

The representative FTIR spectra of QD nanocrystals (A), targeting ligand and drug (B), QD-FA nanocarriers (C) and QD-FA-DOX nanoconjugates (D). The spectra were standardized by a background spectrum determined on the bare KBr substrate.

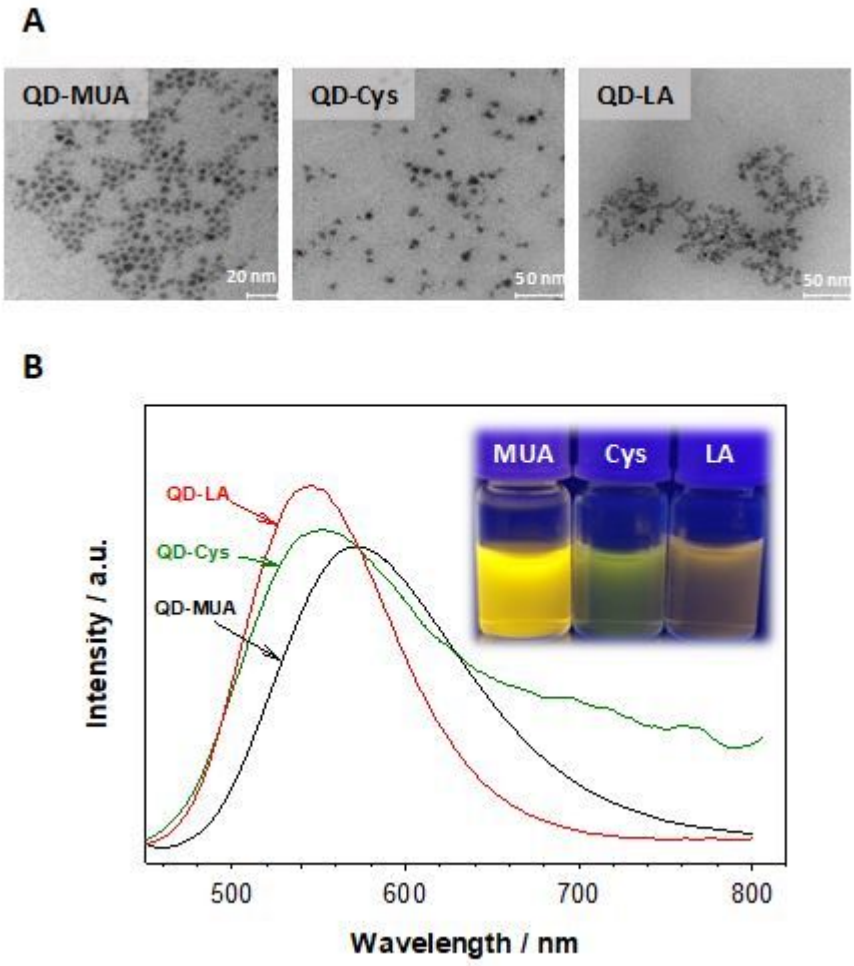

Figure 12

TEM images of QD nanocrystals (A) and their photoluminescence spectra for dispersions in water (B).